Dynamic Thermal Performance of Walls and Ceilings/Attics

K.E. Wilkes
ASHRAE Member

ABSTRACT

The Energy Performance Design System (EPDS) provides a simplified method for predicting annual heating and cooling energy consumption in buildings. This system includes the significant contribution from walls and ceilings. The dynamic thermal performance of walls and ceilings has been studied both by theoretical analyses and by laboratory measurements. The paper gives an overview of laboratory measurement capabilities in this area, consisting of a calibrated hot box for walls and a Thermal Research Facility for measurements on horizontal building elements. An overview is also given of measurement programs that have been performed, including extensions to reduce errors resulting from flanking heat flows. Parallel efforts to improve and validate available analytical models for thermal behavior of walls and ceiling/attic systems are described. These efforts involved comparisons of model predictions with predictions from detailed thermal calculations and results from the measurement programs. Certain of these improvements were incorporated into the analytical models; others continue to be studied. These models were then combined with a balance-point accounting procedure and were used to calculate heating and cooling loads for a wide variety of walls and ceiling/attic configurations that are included in EPDS. Calculated results for various orientations were consolidated and represented algebraically as functions of thermal resistance and heating and cooling degree-days with various base temperatures.

INTRODUCTION

The Energy Performance Design System (EPDS) provides a simplified method for predicting annual heating and cooling energy consumptions in buildings. Walls and ceilings represent a significant contribution to these energy consumptions. A significant amount of research has been performed to develop an understanding of the thermal performance of building envelope elements. This paper summarizes the research performed to date on walls and ceilings/attics and relates this research to the calculation procedures used in the EPDS. Since some of this information has been reported elsewhere,[1-7] this paper will focus on presenting new information.

Research programs conducted on the thermal performance of walls and ceilings/attics consisted of closely coordinated experimental and analytical

K. E. Wilkes, Research and Development Division, Owens-Corning Fiberglas Corporation, Technical Center, Granville, Ohio.

phases. In this way, available analytical models were improved and validated against experimental data obtained under laboratory-controlled conditions. The accuracy of simplified models was also determined by comparison with more detailed models and experimental results.

LABORATORY FACILITIES

Two principal facilities were used to perform laboratory measurements of heat flow through opaque building elements. A calibrated hot box, Fig. 1, was used for vertical wall sections; the Thermal Research Facility, Fig. 2, was used for horizontal ceiling/attic sections. Since the construction of the facilities has been described in detail in Refs 1, 2, and 3, only brief descriptions will be given here.

Calibrated Hot Box

The calibrated hot box allows tests on 9 by 14 ft (2.7 by 4.3 m) wall sections of various thicknesses. The wall is sandwiched between metering and climatic chambers. The metering chamber is usually held at a fixed temperature to represent indoor conditions, and the temperature in the climatic chamber may be maintained at a constant value or may be changed with time in a controlled manner. In this way, either steady-state or dynamic tests simulating various climatic conditions can be performed.

The measured net heat input to the metering chamber must be suitably corrected to determine the amount of heat that actually flows through the test sample. It has long been recognized that corrections must be made for heat that escapes through the walls of the metering chamber. But only recently has it been recognized that other corrections may be needed to account for heat that flows around the test sample through its frame (flanking loss) and for heat that is stored in the thermal mass of the metering chamber during transient tests.

The flanking loss has been studied by a combination of experiments and finite difference analyses, details of which are reported in Ref 4. This work derived the dependence of the flanking heat flow on the sample thickness, temperature difference between the chambers, and the mean temperature for this particular hot box. For a typical insulated wall section, the flanking heat flow may be on the order of 5% of the heat flow through the test sample. Using the flanking calibration reduces the error due to flanking to about the 1% level and thus allows more accurate determinations of the heat flow through more complex test samples.

Calibrated hot boxes have only recently begun to be used for transient tests. Transient calibration tests were performed on specimens made from standard calibration material. These included tests with two specimen thicknesses and with the temperature in the climatic chamber being stepped down, stepped up, and driven through a simulated sol-air cycle. Heat flow through the sample was obtained from the net heat input to the metering chamber after corrections for flanking and box heat losses. Calibrated heat-flux transducers were used to obtain an independent measure of the sample heat flow, as well as the flanking and box losses. A comparison of the two values of sample heat flow showed that an additional correction was needed to account for heat storage in the materials within the metering chamber. The control procedure was to hold the temperature of the airstream constant at the point at which it first started to sweep across the sample. Since the airflow rate was also held constant, downstream temperatures changed whenever the heat flow through the specimen changed. Analysis of the heat capacity of the materials in the metering chamber and the experimental data resulted in an effective metering chamber heat capacity of 140 Btu/^{o}F (266 kJ/K). A correction for heat storage was calculated as the product of this heat capacity and the rate of change of the mean temperature of the metering chamber, as obtained from

thermocouples attached to a solid component within the metering chamber. It was found that this measured value fluctuated significantly, and smoothing techniques were required to obtain meaningful results.

Application of this heat storage correction to the measured heat input resulted in good agreement with the sample heat flows measured directly by heat flow transducers. Identification of this effect has also led to an improvement in the procedure for operating the hot box, whereby the average air temperature is maintained at a constant value. This should reduce temperature fluctuations at all points in the metering chamber and also result in compensation of heat storage at some points with heat releases at other points to give a much smaller net heat storage effect.

Thermal Research Facility

This facility was constructed to allow tests on horizontal building elements such as ceilings and floors. The basic facility consists of a large environmental chamber having a 14 by 20 ft (4.3 by 6.1 m) open area in its floor, below which is a hybrid calibrated-guarded metering chamber. As with the calibrated hot box, the metering chamber is usually held at a fixed temperature to represent indoor conditions. The temperature in the environmental chamber can be controlled from -50 to 150°F (-46 to 66°C), and may be maintained at a constant value or changed with time, to simulate either steady-state or dynamic environmental conditions, respectively. A urethane foam ring with a glass fiber reinforced plastic surface is placed around the top periphery of the metering chamber to act as an insulated sample support. As with the calibrated hot box, a series of tests was performed with a sample of known thermal properties to determine corrections for heat losses through the metering chamber walls and through the support ring. As described in detail in Ref 3, analysis of the data from this series of tests yielded corrections for these two heat flow paths that should allow the heat flow through the sample to be determined to within about 3%. The correction for heat flows through the chamber walls are determined from readings of heat flux transducers placed within the walls; the heat flow through the support ring is determined from the air-to-air temperature difference between the metering and environmental chambers.

MEASUREMENT PROGRAMS

Walls

A matrix of experiments on walls typical of residential construction was laid out to investigate the effect of the following variables: level of insulation, temperature level, and heat storage effects. Five 9 by 14 ft (2.7 by 4.3 m) walls were built. Three were of wood frame construction using 2 x 4 studs, 16 in. (0.41 m) on center. Each wall had a polyethylene vapor barrier and gypsum wallboard on the inside and a sheathing product and redwood lap siding on the outside. One had no insulation in the stud cavities and 1/2-in. (13 mm) regular-density wood fiberboard sheathing. Another wall was identical except that the cavities were filled with R-13* glass fiber insulation. The third frame wall also had R-13 glass fiber insulation in the cavities but had 1-in. (25 mm) glass fiber sheathing rather than wood fiber sheathing. The other two walls were constructed of two-core hollow concrete blocks. One wall was uninsulated; the other was insulated with R-13 glass fiber insulation in the cavities of 2 x 4 studs, 16 in. (0.41 m) on center, and was covered with a vapor barrier and gypsum wallboard.

Each of the walls was instrumented with numerous thermocouples and heat flow transducers. Besides the instrumentation needed to meet the requirements

* Nominal insulation R-values are in IP units: $hr \cdot ft^2 \cdot {}^\circ F/Btu$.

of ASTM C-976, additional instrumentation was installed to allow study of the temperature patterns in more detail. Thermocouples used to measure average surface temperatures were representatively distributed over the studs and cavity centers on the frame walls and over the cores, webs, and joints on the masonry walls. Thermocouples were also used to measure air temperatures at corresponding locations. Other thermocouples were used to measure temperatures at selected points within the interior of the walls.

Three steady-state tests were run on each of the walls. For each test, the indoor air temperature was maintained near 75°F (23.9°C). The outdoor air temperatures for the three tests were nominally -25°F, 25°F, and 150°F (-32°C, -4°C, and 66°C). These temperatures were chosen to simulate sol-air temperatures corresponding to severe winter, typical winter, and severe summer conditions. In addition, transient step-down and step-up tests were conducted while changing from one steady-state condition to another. Additional steady-state tests at -25°F (-32°C) outdoor temperature were performed on the frame walls with the redwood siding removed.

Ceilings/Attics

A 14 by 20 ft (4.3 by 6.1 m) simulated residential attic with a gabled roof was built over the metering chamber of the Thermal Research Facility.[8,9] The attic was built with 2 x 4 raised trusses with 2 x 6 top chords having a pitch of 5 in 12. The ceiling consisted of 5/8-in. (16 mm) gypsum wallboard, and the gables of 1/2-in. (13 mm) wood fiber sheathing. The roof and other vertical sides consisted of 1/2-in. (13 mm) plywood. The attic was ventilated through ridge and eave vents using a blower system. Solar radiation incident on the roof was simulated by electrical heater pads. The attic and insulation were instrumented with thermocouples at several locations and heat flux transducers to measure ceiling heat flows. Thermocouples were placed at all major surfaces and interfaces and in the different air spaces, in excess of the requirements of ASTM C-976.

A matrix of experiments was laid out to investigate the effect of the following variables: level of insulation, temperature level, ventilation rate, solar heating of roof, and heat storage. Among the many types of insulations investigated were no insulation, R-11, R-19, and R-38 glass fiber batts. The R-38 batt insulation was composed of two layers of R-19 batts installed in a crisscross fashion. For each of these insulation levels, experiments were conducted under the five steady-state and two transient conditions listed in Tab. 1. The first two tests represent extreme winter conditions with ventilation rates spanning the range of anticipated natural ventilation rates. For these two tests, no heat was supplied to the roof heaters and, thus, the roof temperature was allowed to seek its own level.

The next three tests represent summer conditions with the roof temperature controlled to a representative sol-air temperature of 150°F (66°C). Representative combinations of outdoor air temperature and ventilation rates were selected to cover a wide range of summer conditions, with ventilation rates ranging from no ventilation to those typical of forced ventilation using an attic fan.

The sixth and seventh tests are transient tests corresponding to winter and summer conditions. For each of these tests, the roof temperature was driven through a sol-air temperature profile calculated for a dark roof at 40° north latitude with the ridge oriented in the east-west direction. For the winter test, only the south roof was driven through a cycle appropriate to Dec. 21; the north roof was allowed to seek its own level, since it would be in the shade. For this test, the outdoor temperature was held constant. For the summer test, both roof surfaces were driven through a cycle appropriate to June 21, while the outdoor temperature was controlled to follow the profile suggested by ASHRAE using a national average of the 1% level design temperature and the daily temperature range. The winter and summer cycles used are given in Figs. 3 and 4.

DEVELOPMENT OF MODELS

Models of the thermal performance of walls and ceilings/attics were developed at various levels of detail. These included parallel path, finite difference, lumped capacity, and response factor calculations. Models for ceilings/attics included those for only the ceiling/insulation system (similar to a wall), as well as models for the entire attic system, including the ceiling, roof, gables, and attic space. Both steady-state and transient models were developed.

Most of the models accounted for the temperature dependence of the thermal conductivity of the materials. The material thermal properties that were used in the models were based on information from the data base project in Ref 7, and are listed in Tabs. 2 and 3. Natural convection in air gaps was modeled using the NBS correlations.[10]

Steady-State Models

The primary model used for steady-state analysis of walls was the parallel path model. This model assumed that the exterior surfaces of the wall were isothermal and, thus, joined the two parallel paths at this point. A mean temperature was calculated for each layer in each path, and the temperature-dependent thermal conductivity of each material was used to obtain thermal resistances for each layer. An iterative procedure was used to obtain a self-consistent solution for the thermal resistance of the wall.

For a few cases, two-dimensional finite-difference calculations were also performed for walls to check the accuracy of the parallel-path model. In addition, three-dimensional finite-difference calculations were performed for the same cases to determine more accurately the influence of metal fasteners.

Steady-state analyses of the ceiling/insulation system relied primarily upon the finite-difference method using a public domain computer program.[11] Two-dimensional analyses were used to calculate detailed temperature patterns and heat flows in a section of the ceiling far from the edges of the attic. Three-dimensional analyses were used to calculate the influence of the attic edges on overall heat flows through the ceiling. A simplified model based on conduction shape factors was also developed for computing the effects of edge heat flows. Edge effects were found to be important for an attic the size of the test attic, but would be less important for sizes in actual residential attics. Full details of these calculations, including the handling of boundary conditions, are given in Ref 6.

Transient Models

Models for the transient thermal performance of walls and ceilings/attics were based primarily on the thermal response factor method.[12,13] The computer program used for calculation of response factors from material thermal properties was obtained from the National Bureau of Standards in 1973; several modifications have since been made to improve the accuracy of the numerical techniques used in this program. In the original derivation of the response factor method, the assumption of temperature-independent thermal properties was made. A method has been devised to incorporate temperature-dependent properties at least in a first-order manner. The accuracy of extensions to the method was assessed by comparison to more basic calculations that could be considered to be exact.

The variable property heat conduction equation may be reduced to a simpler form by introducing a new variable defined as[14]

$$\Theta = \frac{1}{k_R} \int_{T_R}^{T} k \, dT \tag{1}$$

where

k = thermal conductivity at temperature T
k_R = thermal conductivity at T_R
T_R = reference temperature

In terms of this variable, the resulting heat conduction equation is

$$\frac{1}{\alpha} \frac{\partial \Theta}{\partial t} = \frac{\partial^2 \Theta}{\partial x^2} \tag{2}$$

where

α = thermal diffusivity

This equation has the same form as the heat conduction equation for constant properties. If the thermal diffusivity were a constant, solutions of the constant property heat conduction equation may be taken over directly by replacing T by Θ, providing the boundary conditions specify only T or its gradient. Although the thermal diffusivity of building materials is not generally independent of temperature, this approximation is made, and its justification will be determined later.

The derivation of the response factor method for the multilayer composite required that temperature and heat flux be continuous across the boundary between any two layers. The transformation of Eq 1 automatically guarantees continuity of $k_R \, \partial\Theta/\partial x$ across interfaces. However, continuity of Θ across boundaries requires the extra approximation of identical temperature dependences of thermal conductivity among the layers. Assuming a linear temperature dependence, the thermal conductivity of the i^{th} layer may be written as

$$k_i = k_{R,i} \left[1 + \beta_i \, (T - T_R) \right] \tag{3}$$

Continuity of Θ thus requires that all β_i be assumed to be equal.

Having satisfied these conditions, the response factor equations relating the inside surface heat flux to surface temperatures may be written as

$$QI_\tau = \sum_{i=o}^{\infty} X_i \, \Theta I_{\tau - i\delta} - \sum_{i=o}^{\infty} Y_i \, \Theta O_{\tau - i\delta} \tag{4}$$

where

QI_τ = heat flux at time τ at the inside surface of the composite
$\Theta I_{\tau - i\delta}$ = transformed temperature on inside surface at time $\tau - i\delta$
$\Theta O_{\tau - i\delta}$ = transformed temperature on outside surface at time $\tau - i\delta$
X_i and Y_i = response factors calculated in the usual way using properties evaluated at T_R

A similar equation may be written for the heat flux at the outside surface using the Y and Z response factors.

Performing the transformation indicated above gives the following equation for the inside heat flux:

$$QI = \sum_{i=o}^{\infty} X_i \, (TI_{\tau - i\delta} - T_R) - \sum_{i=o}^{\infty} Y_i \, (TO_{\tau - i\delta} - T_R) + \frac{\beta}{2} \left[\sum_{i=o}^{\infty} X_i \, (TI_{\tau - i\delta} - T_R)^2 - \sum_{i=o}^{\infty} Y_i \, (TO_{\tau - i\delta} - T_R)^2 \right] \tag{5}$$

where

$TI_{\tau - i\delta}$ = usual temperature at inside surface
$TO_{\tau - i\delta}$ = usual temperature at outside surface

A similar equation may be written for the outside heat flux.

Application of this relation to steady-state conditions identifies the appropriate value of β as that calculated from the temperature dependence of the overall conductance of the composite. The reference temperature is

arbitrary and may be selected for the problem at hand. For this work, it was chosen to be 75 °F (23.9 °C) to correspond to the usual practice for building heat flow calculations. It should also be noted that even in the temperature-independent response factor method, a reference temperature is usually introduced to decrease numerical errors. In this case, the temperature-independent equations are identical to the temperature-dependent equations with β set equal to zero.

The conduction transfer function equations given in Ref 13 may be extended in a similar fashion. Conduction transfer functions are again calculated at the reference temperature. The resulting equations contain the extra terms involving β and the square of the temperature as in the response factor equation.

Heat transfer calculations in most building elements involve deviations from the one-dimensional conduction assumed in the response factor method. This two-dimensional conduction is usually approximated by dividing the system into parallel paths, using the response factor method to calculate the heat flow through each of the paths separately and then adding the heat flows together.

In a variation on this approach, suggested by Peavy,[15] a set of response factors is constructed for the entire assembly. If the exterior surfaces of the assembly are assumed to be isothermal, the composite response factors may be calculated as the area-weighted average of the response factors of the individual paths.

Peavy also suggested that these composite response factors may be used to develop composite conduction transfer functions in the usual way, providing the proper composite common ratio is used. Assuming that one path is heavier, i.e., has a larger number of significant response factors, the common ratio of the composite response factors will reduce to the common ratio of the response factors for this heavier path. Composite conduction transfer functions may then be calculated using the composite response factors and this common ratio. Simultaneous effects of temperature-dependent properties and two-dimensional conduction may be handled by using composite response factors or conduction transfer functions in conjunction with the temperature dependence of the surface-to-surface conductance of the entire assembly.

The merit of the approximate methods derived here was determined by applying them to three test cases and comparing the results with those of finite-difference calculations. The combined analysis was applied to a typical section of an insulated frame wall, composed of 2 x 4 wood studs, 16 in. (0.41 m) on center, R-11 glass fiber insulation, 1/2-in. (13 mm) gypsum wallboard on the inside, and 1/2-in. (13 mm) wood fiber sheathing and aluminum siding on the outside. For numerical convenience, inside and outside film coefficients were taken to be 1.0 hr·ft^2·°F/Btu (0.18 m^{2}K/W). The thermal resistance of the aluminum siding was added to the outside film resistance, and the sum was treated as an effective outside resistance. The temperature of the air on the inside was held constant at 75 °F (23.9 °C), and the outside air temperature varied sinusoidally between 0 °F (-17.8 °C) and 75 °F (23.9 °C) with a period of 24 hr. In addition to this two-dimensional case, the stud and insulation paths were treated independently.

The material properties used in the calculations were similar to those given in Tabs. 2 and 3. Response factors were evaluated at 75 °F (23.9 °C) and values of β were determined from steady-state finite difference (2-D) or hand calculations (1-D) with inside and outside temperatures of 75 °F (23.9 °C) and 0 °F (-17.8 °C). Values of β were calculated to be 2.8 x 10^{-3}, 3.1 x 10^{-3}, and 1.2 x 10^{-3} °F^{-1} (5.0 x 10^{-3}, 5.6 x 10^{-3}, and 2.2 x 10^{-3} °C^{-1}) for the two-dimensional composite, the insulation path, and the stud path, respectively. The transient finite difference calculations were performed with the HEATING5 program using the Crank-Nicolson method with a time step of 0.1 hours. The nonlinear terms introduced into the temperature-dependent response factor equations required an iterative method of solution. For both types of calculations, the cyclic boundary conditions were applied for a length of time

sufficient to allow initial transients to die out so that all that was left was the steady-periodic response.

These calculation methods are compared in Tab. 4 on the basis of both the peak heat flux and the daily total heat flow. Consider first the one-dimensional, temperature-independent calculations for which an exact solution is also available. For both paths, the peak heat fluxes and daily total heat flows from the finite-difference calculations are nearly identical to those from the exact solution. The response factor calculations tended to round off the peaks slightly (by less than 1.5%) but predicted daily totals nearly identical to the exact solution.

For the one-dimensional, temperature-dependent calculations, no exact solution is available, but, judging from the temperature-independent results, the finite-difference calculations may be considered to be nearly exact. The effect of the temperature-dependent properties is to reduce both the peak and daily total heat flows. Tab. 4 shows that the temperature-dependent response factor calculations are in very good agreement with the finite difference calculations. For both paths, the peak heat flows are within 1.5% and the daily totals are within 0.2%.

For the two-dimensional case, an exact solution is not available for either temperature-dependent or independent properties. Again, the finite difference calculations are considered to correspond to an exact solution. A comparison of the calculations for the complete cycle is shown in Fig. 5. The agreement between the two methods of calculation is good, with the peak heat fluxes agreeing to within about 2.5% and the daily totals being nearly identical.

These comparison calculations lend a good deal of confidence in the extensions to the response factor method when applied to frame walls. There is somewhat less confidence in the applicability of the methods to building elements of much different construction, such as masonry walls.

Attic Models

Models for the overall attic require the coupling of heat flows through several surfaces, as well as with the air within the attic enclosure. A review of available attic models is given in Ref 5. Here, attention will be focused on the models that were used for comparisons with measured data.

The attic model shown in Fig. 6 was developed in the OSU-EPRI project[16,17] and was the model originally adopted by the author's laboratory for transient modeling of attics. A lumped-parameter approach is taken, with the various components being represented as thermal resistances and capacitances. The attic air is assumed to be well-mixed. All heat transfer coefficients are assumed to be the constant values recommended by ASHRAE for design purposes. Heat transfer by radiation within the attic enclosure is not treated separately but is combined with the convection heat transfer coefficients. The model is used in a two-step process. In the first step, the ceiling-insulation system is represented by a thermal resistance with no heat capacity. This step results in a calculated attic air temperature. In the second step, the history of calculated attic air temperatures is used in conjunction with the response factor method to calculate the heat flow through the ceiling-insulation system. It is in this second step that the heat capacity of the ceiling-insulation system is accounted for.

As a result of the work in developing the more sophisticated models (discussed later), it was recognized that the treatment of radiation heat transfer in the OSU-EPRI model was not adequate. To better approximate this process, the model was modified to allow direct radiation exchange between the lower surface of the roof and the upper surface of the ceiling-insulation system. Radiation exchange was modeled using the parallel-plate equation, with a temperature-dependent coefficient being calculated using the surface temperatures calculated at the previous hour of the transient. This was felt

to provide a reasonable approximation while avoiding a time-consuming iterative solution. The model in this form is labeled the OCF-2 model.

A more sophisticated model, shown schematically in Fig. 7, was developed, using Peavy's model as a starting point.[18] The model actually includes seven distinct surfaces (two roofs, two gables, two vertical sides along the eaves, and one ceiling), but, to avoid confusion, the schematic shows only three. Each of the surfaces was represented by conduction transfer functions using the temperature-dependent methodology described earlier. A complete radiation exchange analysis of the enclosure was performed, assuming opaque gray diffuse isothermal surfaces with emittances of 0.9. Each of the surfaces exchanged heat with the attic air by convection. Natural convection coefficients were based on the correlations recommended by Holman.[19] They accounted for the orientation and size of the surface, direction of heat flow, and the instantaneous temperature difference between the surface and the air. In most cases, natural convection was assumed to be turbulent, but, for horizontal or nearly horizontal surfaces with heat flowing in the downward direction, the correlations correspond to laminar flow. Forced convection coefficients were also calculated using an estimate of the air velocity through the attic and assuming turbulent flow. The larger of these two coefficients was selected for the calculations (see Ref 20). The resulting set of nonlinear equations was solved iteratively to predict surface and air temperatures and heat flows. In addition, the heat flow through the ceiling was corrected for edge effects in a quasi-steady manner by applying the corrections described earlier. Two versions of this model were used. In one, the attic air was assumed to be well-mixed; in the other, the attic air temperature was assumed to increase along its flow path.

EXPERIMENTAL RESULTS AND COMPARISON TO MODEL PREDICTIONS

The primary experimental results from steady-state tests were surface-to-surface thermal resistances. For attics, this consisted of the resistance of the ceiling-insulation system only. It included the effects of heat flows at the edges of the attic but did not include the resistance of the attic air space or the roof. Attic air temperatures and total ceiling heat flows were also important results from the steady-state tests and were the primary results for the transient tests.

Walls

Although both steady-state and transient tests have been performed on walls, only the steady-state tests have been analyzed in detail thus far. A summary of the results of steady-state wall tests is given in Tab. 5. It also gives R-values that were predicted by the parallel-path model. With some exceptions, the model predictions are in good agreement with the experimental results. For the 18 tests, the average difference between prediction and experiment is about 8%.

The greatest differences between measurement and prediction occurred for the uninsulated concrete block wall, where the predicted R-values were 15 to 20% higher than the measured values. Predictions using a two-dimensional finite-difference calculation were within 3% of the parallel-path prediction, indicating that the assumption of isothermal exterior surfaces in the parallel-path method was justified. Possible reasons for the discrepancy between prediction and measurement include uncertainties in the thermal conductivity of the concrete and the idealized treatment of radiation and convection within the hollow cores. Radiation was calculated from the infinite parallel-plate equations; real radiation exchanges in the cores of concrete blocks are much more complicated. Natural convection was calculated from correlations that were developed for enclosures similar to cavities in a frame wall and may not be adequate for the geometry of the cores.

The remaining discrepancies over 10% all occurred for the tests at high mean temperatures. For the low mean temperature tests, the calibrated hot box was operated under favorable conditions, with the metering chamber maintained near 75 °F (23.9 °C) and only heating supplied. For the high mean temperature tests, different conditions were used. In some cases, the outside surface of the wall faced the metering chamber, which was maintained at a high temperature with only heating being supplied. In other cases, the inside surface of the wall faced the metering chamber which was maintained near 75 °F (23.9 °C) by a combination of heating and cooling. Although results of both methods were equivalent, the discrepancies between measurement and prediction may be due to experimental errors resulting from various combinations of: (1) uncertainties in the box and flanking calibrations when the metering chamber is at a temperature higher than that of the surrounding laboratory space, and (2) uncertainties in the measurement of net heat flow obtained as the difference between cooling and heating in the metering chamber.

If the results at high temperatures and on the uninsulated block wall are disregarded, the maximum and average differences between measurement and prediction for the remaining 11 tests are 7.5 and 4%, respectively. Three-dimensional finite-difference calculations have shown that part of these discrepancies may result from underestimation by the parallel-path model of conduction by metal fasteners. However, adjustment for this effect does not consistently improve the agreement between measurement and prediction. Thus, with the exception of the uninsulated block wall and the high mean temperature tests, the parallel-path model is able to predict the measured R-values for walls to within about ± 7.5%.

Attics

The primary results of the steady-state attic experiments are the surface-to-surface thermal resistance of the ceiling-insulation system, the heat flow through the ceiling, and the average attic air temperature. These results, along with the experimental conditions, are summarized in Tab. 6. The average attic air temperatue corresponds to measurements 4 in. (100 mm) above the top surface of the insulation.

Measured values were compared with two levels of predictions. The first level of prediction was based on finite-difference calculations, along with the approximate edge correction factors discussed earlier. For these calculations, the boundary conditions were measured values of the air temperature below the gypsum wallboard, the air temperature above the insulation, the air temperature outside the attic, the temperature of the metering chamber surface that faced the ceiling, and the mean radiant temperature seen by the top of the insulation. This mean radiant temperature was based on temperatures measured on the bottom surface of the roof and the inside surfaces of the gables. The second level of prediction was based on the overall attic models. Boundary conditions for these calculations were the same as those mentioned earlier except the measured outside roof temperature and ventilation rate were used instead of the measured attic air temperature and mean radiant temperature. With the second level of prediction, the attic air temperature was predicted.

Since results of the finite-difference models have been discussed in detail in Ref 6, only a brief summary will be presented here. Measured R-values and ceiling heat flows are compared with predictions of the finite-difference models in Tab. 7. For the most important cases of the R-19 and R-38 insulations, the models predicted the measured R-values to within less than 7%. This is considered to be very satisfactory agreement for such a complex heat transfer system. The reason for low predicted R-values for the uninsulated cases was traced to the use of too high a thermal conductivity for gypsum wallboard in the models. Later measurements on a sample of the wallboard gave a thermal conductivity about 20% lower than that used in the model. The discrepancies for the R-11 cases have not been resolved.

Similar agreement was obtained between the predicted and measured heat flows. For the uninsulated cases, the heat flows are actually in better

agreement than the R-values. For the calculation of heat flow, the film resistances are also important, making uncertainties in the thermal conductivity of the gypsum wallboard of less importance than for the calculation of ceiling R-value. For the summer tests on the R-19 insulation, the agreement on heat flows is not as good as that on R-values. For these tests, the roof was heated, and it is possible that nonuniform roof temperatures were produced such that the mean radiant temperatures used in the models were not sufficiently accurate to predict heat flows. Uncertainties in actual temperature levels are less important for modeling the thermal resistance since temperature differences are divided out.

Results of the steady-state attic experiments are compared with predictions of the overall attic models in Tab. 8. With these models, both the ceiling heat flow and the average attic air temperature could be predicted. The two models labeled "air well-mixed" and "air not well-mixed" refer to the enhanced OCF model that includes temperature-dependent response factors, a complete radiation exchange analysis, variable convection coefficients, and edge loss corrections. From Tab. 8, it is seen that these two models and the OCF-2 model all produce reasonably similar predictions of ceiling heat flow. On the other hand, the heat flow predictions of the OSU-EPRI model are usually low. It is difficult to choose one of the three models as being clearly superior. The two enhanced models would be expected to produce the best predictions, but, on the average, the OCF-2 model gives somewhat better predictions. This may be somewhat fortuitous because of compensation of different approximations in this model. If the heat flows predicted by the overall models were compared to those predicted by the finite-difference calculations, the two enhanced models would be somewhat superior to the OCF-2 model. It appears that the model that does not assume the attic air to be well-mixed usually makes better predictions than the one that assumes the condition of well-mixed air. This model usually predicts the ceiling heat flow to within about 10% which is considered quite satisfactory.

Typical results of the transient tests are given in Figs. 8 through 10. These figures show the measured and predicted ceiling heat flows and attic air temperatures over two complete daily cycles. Summer transient tests were chosen for illustration because nearly the entire test is cyclic, whereas the winter case has a smaller cycle superimposed on a steady-state background. It should also be noted that the cycles shown for the R-19 and R-38 cases start at different points, and the curves shown should not be interpreted as indicating a large phase shift between these two cases. These results show that the overall models do a very reasonable job of tracking the transient response of the attic. Again, the three OCF models are in better agreement with the measurements than is the OSU-EPRI model.

Table 9 compares measurements with model predictions for all eight transient tests. Here, the comparisons are based on the ceiling heat flow integrated (on an absolute value basis) over the last 48 hours of the tests (thus representing two complete daily cycles). An integration of absolute values was chosen because the ceiling heat flow changed directions during some of the tests. For the summer test on the uninsulated case, the cycle shown in Fig. 4 could not be followed because of cooling equipment capacity limitations. Instead, the roof temperature was cycled above and below the indoor temperature. Again, the model predictions are in very reasonable agreement with the measured values, with the OCF-2 model and the model that assumes non-well-mixed attic air producing the best predictions. For these models, the predicted integrated ceiling heat flows usually agree with the measured values to within about 10%.

EPDS MODELS

The goal of the EPDS was to provide a simplified method of predicting annual heating and cooling energy consumptions in buildings. It was desired that the simplified method be applicable to a wide variety of walls and ceilings/attics

and a wide range of climatic conditions. Because of the large computational efforts required to determine annual performance for these many combinations of constructions and climates, it was necessary to adopt models that had a proper balance of accuracy, speed, and flexibility. Because of this, not all of the model developments discussed here could be utilized. This section will describe the features of the models that were actually used.

The conduction transfer function (CTF) method was used for both walls and ceilings. The analyses presented earlier show that this method produces results that agree very well with more exact calculations, even when the method is extended to include the temperature dependence of the wall conductance and heat flow through parallel paths. Peavy's method of developing composite CTFs for parallel paths was adopted since computational times would be much shorter than those required when using separate CTFs for each path. The temperature-dependent CTFs were not adopted for two reasons. First, the temperature-dependent CTF method requires an iterative solution for each time step (hourly) and thus would greatly increase computational times. Second, the method requires reliable information on the temperature dependence of the conductance of the wall or ceiling. Although this information was available for some constructions, it was not available for all of them. Therefore, to be equitable, the temperature-dependent method was not applied to any of the constructions.

The most generally applicable models for gabled attics are considered to be the extensions of Peavy's model, the predictions of which were in very reasonable agreement with the results of the attic experiments. However, a much less complicated OCF-2 model was also found to be in reasonable agreement with the experiments. Because of the complications built into the extensions of Peavy's model, an iterative solution is required at each (hourly) time step. Approximations were built into the OCF-2 model so that iterations were not required. Thus, because of its speed as well as its accuracy, the OCF-2 model was chosen for use in the EPDS calculations.

Hour-by-hour external conditions applied to these models were obtained from Test Reference Year (TRY) weather tapes, which specify outdoor dry-bulb temperature, wind speed, and average cloud cover. Outside film coefficients and attic ventilation rates were calculated from the wind speed. Solar insolation was calculated from standard procedures similar to those used in the National Bureau of Standards Load Determination (NBSLD) computer program. The solar absorptances of all walls were taken to be 0.5 and those of all roofs were taken to be 0.85. Indoor conditions were assumed to remain constant, with the air temperature being maintained at 73 ^{o}F (22.8 ^{o}C). The interior surface of the envelope element was assumed to exchange heat by radiation with surfaces that were also at 73 ^{o}F (22.8 ^{o}C). Thus, the interior convection and radiation coefficients could be lumped together into effective film coefficients. ASHRAE-recommended design film coefficients were used, with proper account being taken of the direction of heat flow.

The parallel-path model for walls included the band joist (sometimes called the floor header and end joists). The area fraction for the band joist was taken to be 0.09, corresponding to an 8 ft (2.4 m) wall with a 9.5 in. (0.24 m) band joist. The remainder of the area for frame walls was considered to be made up of framing and insulation paths. The area fractions for these paths were obtained from considerations of typical framing requirements, including studs and window and door frames. For concrete block walls, the remainder of the area was apportioned between web and core paths. For block walls with framing and insulation, the framing was assumed to fall over the webs, dividing the web path into two separate paths corresponding to the insulation and framing.

For the attic model, the ceiling dimensions were taken to be 30 by 40 ft (9.1 by 12.2 m), with the longer dimension oriented in an east-west direction. The gables were taken to be on the east and west ends. Various roof pitches and ceiling constructions were analyzed, but the roof and gables were always assumed to have thermal resistances of 1.2 and 2.8 hr·ft^{2}·^{o}F/Btu (0.21 and 0.49 m^{2}K/W), respectively.

The models were used to calculate heat flows through the building elements for each hour of the year. The hourly heat flows were classified as heat gains or heat losses, depending on the direction of heat flow. Under many conditions, when an individual wall or ceiling is experiencing a heat loss or gain, the entire house will also be experiencing a net heat loss or gain. However, conditions do arise when a wall or ceiling may be experiencing a heat loss while the entire house is experiencing a net heat gain. In this case, the heat loss through the wall or ceiling would be acting to remove some of the heat gain from the other components. This heat loss through the wall or ceiling should not be counted as a contribution to the annual heating load but rather should be counted as a decrease in the annual cooling load due to this component. The inverse case would also be present during some hours of the year.

The allocation of the hourly heat losses and gains was determined by the balance-point accounting procedure described by McBride.[21] With this procedure, the entire house is assumed to be experiencing a net heating load if the outdoor temperature is below the balance point and to be experiencing a net cooling load if the temperature is above the balance point. Therefore, for a given component, the net annual heating load is equal to the sum of the hourly heat losses when the outdoor temperature is below the balance point minus the sum of the hourly heat gains when the temperature is also below the balance point. Likewise, the net annual cooling load is equal to the sum of the hourly heat gains minus the sum of the hourly heat losses, all when the outdoor temperature is above the balance point. The total load from the wall or ceiling is then the sum of the net annual heating and cooling loads. For details on the method of assigning a balance point to a particular building element, see Ref 21.

EPDS RESULTS

The models described here were used to analyze annual heating and cooling loads for a wide range of wall and ceiling/attic constructions and for a wide range of climatic conditions. A total of 143 different residential wall constructions and 99 different ceiling/attic constructions were analyzed. Analyses for walls were performed for east, west, north, and south orientations. Since there were no major differences among the various orientations, the results were averaged together. The walls included both wood frame and concrete block constructions. Some walls were of conventional construction such as 2 x 4 frame walls with R-11 insulation in the cavities and 2 x 6 frame walls with R-19 cavity insulation. These same walls were also analyzed with various levels of interior or exterior insulating sheathing. Other more energy-efficient constructions used double stud walls or truss walls with insulation levels ranging as high as R-54. Similarly, the concrete block walls analyzed included uninsulated walls as well as walls insulated on either the interior or exterior surfaces. Likewise, both conventional and energy-efficient ceiling/attics were analyzed. These included several types of trusses, some of which allow for 1 to 2 ft of insulation at the eaves. Insulation levels ranged from R-11 to R-76. In addition, plank and beam ceilings were analyzed.

Each of these constructions was analyzed using weather data for Bismarck, Minneapolis, St. Louis, Ft. Worth, and Miami. The totals of annual heating and cooling loads were cast in a per-unit area basis and were termed energy factors. The weather data for each of the cities were analyzed to determine the number of heating and cooling degree-days for various base temperatures. For each family of construction (i.e., sets of construction types differing only in overall R-value), regression analyses were performed to obtain equations for heating and cooling energy factors as functions of the component U-value, the house balance point, the number of heating and cooling degree-days for various base temperatures, and the number of cooling hours over 80 °F (26.7 °C). The forms of the regression equations developed in this manner are

given in Tab. 10. The effect of energy storage in the component was taken into account in this analysis by deriving separate regression equations for each family of construction. As noted earlier, these results were derived under conditions of a constant indoor temperature. The refinement of accounting for energy storage under conditions of floating indoor temperature has not yet been incorporated into EPDS.

The final application of these results is to estimate the total seasonal loads for an entire house. The energy factors described here give the seasonal loads per unit area for an individual component under a fixed indoor temperature of 73°F (22.8°C). To estimate the total seasonal loads for an entire house, the individual energy factors are multiplied by the appropriate areas and are then summed over all the components of the house. Finally, these total house loads are adjusted for other thermostat settings, e.g., 68°F (20.0°C) for heating and 78°F (25.6°C) for cooling, by applying the procedure described in Ref 21.

SUMMARY

A significant amount of research has been performed on the thermal performance of walls and ceiling/attics. This research involved advances in analytical techniques as well as experimental investigations. A solid foundation was built for the development of a simplified technique for analyzing these building elements.

The complex thermal performance of each type of building element has been reduced to two nonlinear algebraic equations that relate annual heating and cooling loads to the thermal resistance of the component, the number of heating and cooling degree-days, the number of cooling hours, and the house balance point. Using these simplified equations, along with similar ones for the remaining elements of a building, the annual thermal performance of a complete building may be quickly analyzed.

ACKNOWLEDGMENTS

The author wishes to acknowledge the contributions of several people to the work reported here. Adrienne Lavine coordinated the wall research program and performed much of the analysis related to the test walls and to the performance of the calibrated hot box. She also performed the initial analyses for the EPDS. Clarke Berdan II and Larry Brand performed the final analyses for EPDS. James Rucker was responsible for performance of the experiments on both walls and ceiling/attics. Kenneth Koehler was the technician who built the test sections and assisted in performing the experiments. Richard Godfrey and John Mumaw provided overall supervisory guidance.

REFERENCES

1. J. R. Mumaw, "Calibrated Hot Box: An Effective Means for Measuring Thermal Conductance in Large Wall Sections," Heat Transfer Measurements in Thermal Insulations, ASTM STP 544 (Philadelphia, PA: American Society for Testing and Materials, 1974), p. 193-211.

2. J. R. Mumaw, "Thermal Research Facility--A Large Calibrated Hot Box for Horizontal Building Elements," Thermal Insulation Performance, ASTM STP 718, eds. D. L. McElroy and R. P. Tye (Philadelphia, PA: American Society Testing and Materials, 1980), p. 195-207.

3. J. L. Rucker and J. R. Mumaw, "Calibration Procedures and Results for a Large Calibrated Hot Box," Proceedings of the ASHRAE/DOE-ORNL Conference, Thermal Performance of the Exterior Envelopes of Buildings, ASHRAE SP 28 (New York, NY: ASHRAE, 1981), p. 237-249.

4. A. G. Lavine, J. L. Rucker, and K. E. Wilkes, "Flanking Loss Calibration for a Calibrated Hot Box," Thermal Insulation, Materials, and Systems for Energy Conservation in the '80's, ASTM STP 789, eds. F. A. Govan, D. M. Greason, and J. D. McAllister (Philadelphia, PA: American Society for Testing and Materials, 1983), p. 234-247.

5. K. E. Wilkes, "Modeling of Residential Attics," Proceedings of the ASHRAE/DOE-ORNL Conference, Thermal Performance of the Exterior Envelopes of Buildings, ASHRAE SP 28 (New York, NY: ASHRAE, 1981), p. 436-455.

6. K. E. Wilkes and J. L. Rucker, "Thermal Performance of Residential Attic Insulation," to be published in Energy and Buildings (Lausanne, Switzerland: Elsevier Sequoia, S. A.).

7. K. E. Wilkes, "Thermophysical Properties Data Base Activities at Owens-Corning Fiberglas," Proceedings of the ASHRAE/DOE-ORNL Conference, Thermal Performance of the Exterior Envelopes of Buildings, ASHRAE SP 28 (New York, NY: ASHRAE, 1981), p. 662-677.

8. Wilkes, Residential Attics, p. 436-455.

9. Wilkes and Rucker, Energy.

10. H. E. Robinson, F. J. Powlitch, and R. S. Dill, "The Thermal Insulating Value of Airspaces," Housing and Home Finance Agency, Housing Research Paper No. 32 (Washington, DC: U. S. Government Printing Office, 1954).

11. W. D. Turner, D. C. Elrod, and I. I. Simon-Tov, HEATING5--An IBM 360 Heat Conduction Program, ORNL-CSD-TM-15 (Oak Ridge, TN: Oak Ridge National Laboratory, Nuclear Division, Union Carbide Corporation, 1976).

12. T. Kusuda, "Thermal Response Factors for Multi-Layer Structures of Various Heat Conduction Systems," ASHRAE Transactions 75 (1969), 1:246-271.

13. B. A. Peavy, "A Note on Response Factors and Conduction Transfer Functions," ASHRAE Transactions 84 (1978), 1:688-690.

14. H. S. Carslaw and J. C. Jaeger, Conduction of Heat in Solids, 2nd ed. (Oxford, England: Oxford University Press, 1959), p. 10-11.

15. B. A. Peavy to K. E. Wilkes, 1979.

16. "Fuel Utilization in Residential Heating," Project 460X Final Report (Columbus, Ohio: The Ohio State University Engineering Experimentation Station, 1977).

17. R. S. Blancett et al, "A Model for Predicting Residential Attic Space Air Temperatures," ASHRAE Transactions 85 (1979), 1:656-663.

18. B. A. Peavy, "A Model for Predicting the Thermal Performance of Ventilated Attics," Summer Attic and Whole-House Ventilation, NBS Spec. Pub. 548 (Washington, DC: National Bureau of Standards, 1979), p. 119-145.

19. J. P. Holman, Heat Transfer, 4th ed. (New York: McGraw-Hill Book Co., Inc., 1976), p.245-272.

20. J. R. Lloyd and E. M. Sparrow, "Combined Forced and Free Convection Flow on Vertical Surfaces," Int. J. Heat and Mass Transfer 13 : 2 (Feb. 1970), p. 434-438.

21. M. F. McBride, "Development of a Simplified and Manual Energy Calculation Procedure for Residences" (Paper presented at the Conference on Thermal Performance of the Exterior Envelopes of Buildings II, Las Vegas, NV, Dec., 1982).

TABLE 1

Matrix of Attic Tests

Test No.	Type	Temperature Conditions, °F (°C) Ambient	Roof	Forced Ventilation Rate, cfm/ft^2 (m/s)
1	Steady-state	0 (-18)	Floating	0 (0)
2	Steady-state	0 (-18)	Floating	0.5 (0.0025)
3	Steady-state	80 (27)	150 (66)	0 (0)
4	Steady-state	90 (32)	150 (66)	0.5 (0.0025)
5	Steady-state	100 (38)	150 (66)	1.5 (0.0076)
6	Transient	0 (-18)	Winter sol-air cycle	0 (0)
7	Transient	Summer daily cycle	Summer sol-air cycle	0.5 (0.0025)

TABLE 2

Thermal Properties of Construction Materials*

Material	Density, lb/ft^3 (kg/m^3)	Moisture, %	Thermal Conductivity W/(m·K)	Thermal Conductivity Btu·in/(hr·ft^2·$^\circ$F)	Specific Heat kJ/(kg·K)	Specific Heat Btu/(lb·$^\circ$F)
Wood (attic)	28 (450)	8	$0.1057 + 3.121 \times 10^{-4}T$	$0.6941 + 1.202 \times 10^{-3}T$	$1.395 + 5.465 \times 10^{-3}T$	$0.3099 + 7.252 \times 10^{-4}T$
Plywood (attic)	34 (545)	9	$0.1255 + 2.032 \times 10^{-4}T$	$0.8453 + 7.827 \times 10^{-4}T$	$1.420 + 5.668 \times 10^{-3}T$	$0.3152 + 7.521 \times 10^{-4}T$
Wood fiber sheathing (attic)	19 (305)	-	$0.05375 + 1.303 \times 10^{-4}T$	$0.3566 + 5.018 \times 10^{-4}T$	$1.112 + 4.911 \times 10^{-3}T$	$0.2447 + 6.516 \times 10^{-4}T$
Gypsum wallboard	43 (690)	-	$0.150 + 3.001 \times 10^{-5}(T-41.8)^2$ for $T<41.8^\circ$C 0.150 for $T>41.8^\circ$C	$1.04 + 6.421 \times 10^{-5}(T-107.3)^2$ for $T<107.3^\circ$F 1.04 for $T>107.3^\circ$F	$1.036 + 1.849 \times 10^{-3}T$	$0.2396 + 2.453 \times 10^{-4}T$
Wood (walls)	30 (480)	7	$0.1100 + 3.235 \times 10^{-4}T$	$0.7229 + 1.246 \times 10^{-3}T$		
Wood fiber sheathing (walls)	19 (309)	-	$0.05422 + 1.308 \times 10^{-4}T$	$0.3598 + 5.038 \times 10^{-4}T$		
Fiberglas sheathing (walls)		-	$0.03288 \exp[0.00423(T-23.9)]$	$0.228 \exp[0.00235(T-75)]$		
Concrete	117 (1880)	-	$1.186 - 2.653 \times 10^{-3}T$	$8.5488 - 0.01022\,T$		
Metal fasteners		-	44.7	310.		

* See Ref 10.

TABLE 3

Thermal Properties of Batt Insulation Materials*

Nominal R-Value	Installed Thickness, inches (mm)	Installed Bulk*** Density, lb/ft^3 (kg/m^3)	Thermal Conductivity, W/(m.K)	Thermal Conductivity, Btu·in/(hr·ft^2·°F)	Specific Heat, kJ/(kg·K)	Specific Heat, Btu/(lb·°F)
R-11	3.5** (89)	0.615 (9.85)	$0.04729 \exp[0.007011(T-23.9)]$	$0.3279 \exp[0.003895(T-75)]$	$0.7741 + 1.294 \times 10^{-3}T$	$0.1794 + 1.717 \times 10^{-1}T$
R-19	5.5 (140)	0.687 (11.0)	$0.04563 \exp[0.006658(T-23.9)]$	$0.3164 \exp[0.003699(T-75)]$	$0.7741 + 1.294 \times 10^{-3}T$	$0.1794 + 1.717 \times 10^{-4}T$
R-30	10.25 (260)	0.738 (11.8)	$0.04471 \exp[0.006449(T-23.9)]$	$0.3100 \exp[0.003583(T-75)]$	$0.7741 + 1.294 \times 10^{-3}T$	$0.1794 + 1.717 \times 10^{-4}T$
R-13	3.5 (89)	0.975 (15.6)	$0.04038 \exp[0.005765(T-23.9)]$	$0.2800 \exp[0.003203(T-75)]$	$0.7741 + 1.294 \times 10^{-3}T$	$0.1794 + 1.717 \times 10^{-4}T$

* See Ref 10.

** Estimated.

*** For transient calculations, the mass of air enclosed with the insulation was accounted for by adding 0.075 lb/ft^3 (1.2 kg/m^3) to the bulk density.

TABLE 4

Comparison of Methods of Calculation of Inside Heat Flow
For Insulated Frame Wall Under Cyclic Boundary Conditions

	Insulation Path		Stud Path		2-D Wall Section	
Peak Heat Flux, Btu/(hr·ft^2) (W/m^2)						
Temperature-independent						
Exact	4.84	(15.27)	7.24	(22.84)	-	(-)
Finite-difference	4.84	(15.27)	7.24	(22.84)	5.10	(16.09)
Response factors	4.77	(15.05)	7.18	(22.65)	4.97	(15.68)
Temperature-dependent						
Finite-difference	4.38	(13.82)	7.11	(22.43)	4.70	(14.83)
Response factors	4.33	(13.66)	7.02	(22.15)	4.58	(14.45)
Daily Total Heat Flow, Btu/ft^2 (Wh/m^2)						
Temperature-independent						
Exact	58.56	(184.73)	103.44	(326.31)	-	(-)
Finite-difference	58.58	(184.80)	103.52	(326.56)	63.51	(200.35)
Response factors	58.57	(184.76)	103.52	(326.56)	63.50	(200.32)
Temperature-dependent						
Finite-difference	54.34	(171.42)	101.43	(319.97)	59.59	(187.98)
Response factors	54.43	(171.70)	101.47	(320.10)	59.59	(187.98)

TABLE 5

Comparison of Predicted and Measured Wall Thermal Resistances

Test	Mean Temp., °F (°C)	Measured R-Value (hr·ft²·°F)/Btu [m²·K/W]	Predicted R-Value** (hr·ft²·°F)/Btu [m²·K/W]	Percent Difference (Predicted-Measured)
Uninsulated Frame	26.5 (-3.1)	2.78 (0.490)	* 2.89 (0.509)	4.0
	27.0 (-2.8)	3.76 (0.662)	3.86 (0.680)	2.7
	50.5 (10.3)	3.60 (0.634)	3.73 (0.657)	3.6
	114.5 (45.8)	3.32 (0.585)	3.28 (0.578)	-1.2
Frame R-13	26.0 (-3.3)	13.80 (2.430)	* 13.30 (2.340)	-3.6
	27.3 (-2.6)	14.60 (2.570)	14.30 (2.520)	-2.1
	50.4 (10.2)	13.80 (2.430)	13.50 (2.380)	-2.2
	102.0 (38.9)	10.70 (1.880)	11.80 (2.080)	10.3
Frame R-13 + Insulating Sheathing	25.2 (-3.8)	16.50 (2.910)	* 17.50 (3.080)	6.1
	24.4 (-4.2)	17.40 (3.060)	18.50 (3.260)	6.3
	50.5 (10.3)	16.10 (2.840)	17.30 (3.050)	7.5
	106.8 (41.6)	13.00 (2.290)	14.80 (2.610)	13.8
Uninsulated Block	32.7 (0.4)	1.04 (0.183)	1.22 (0.215)	17.3
	52.6 (11.4)	1.07 (0.188)	1.23 (0.217)	15.0
	109.4 (43.0)	0.98 (0.173)	1.17 (0.206)	19.4
Block R-13	25.4 (-3.7)	13.60 (2.400)	13.80 (2.430)	1.5
	49.2 (9.6)	12.60 (2.220)	13.00 (2.290)	3.2
	108.8 (42.7)	9.30 (1.640)	11.10 (1.950)	19.4

* Test conducted with no siding on wall.
** Parallel path.

TABLE 6

Results of Steady-State Attic Experiments***

	Test	Temperature Conditions, °F (°C) Roof	Outside	Inside	Ventilation Rate, cfm/ft² (m/s)	Measured** Ceiling Heat Flow, Btu/hr (W)	Measured System Thermal Resistance, (hr·ft²·°F)/Btu [m²·K/W]	Measured Attic Air Temperature, °F (°C)
R-0	1	19 (-7)	0 (-18)	75 (24)	0 (0)	6526 (1913)	0.585 (0.103)	36.1 (2.3)
	2	13 (-11)	0 (-18)	74 (23)	0.5 (0.0025)	9013 (2641)	0.617 (0.109)	17.6 (-8.0)
	3	114 (46)	81 (27)	75 (24)	0 (0)	-3103 (-909)	0.648 (0.114)	93.7 (34.3)
	4	113 (45)	90 (32)	75 (24)	0.5 (0.0025)	-2759 (-809)	0.680 (0.120)	93.4 (34.1)
	5	106 (41)	101 (38)	75 (24)	1.5 (0.0076)	-2942 (-862)	0.685 (0.121)	97.2 (36.2)
R-11 Batts	1	3 (-16)	-3 (-19)	75 (24)	0 (0)	1776 (520)	9.47 (1.67)	7.3 (-13.7)
	2	1 (-17)	-3 (-19)	75 (24)	0.5 (0.0025)	1848 (542)	9.79 (1.72)	1.3 (-17.1)
	3	156 (69)	79 (26)	77 (25)	0 (0)	-1300 (-381)	11.19 (1.97)	131.6 (55.3)
	4	148 (64)	89 (32)	77 (25)	0.5 (0.0025)	-1125 (-330)	9.12 (1.61)	109.8 (43.2)
	5	151 (66)	101 (38)	77 (25)	1.5 (0.0076)	-1181 (-346)	9.41 (1.66)	115.2 (46.2)
R-19 Batts	1	6 (-14)	1 (-17)	75 (24)	0 (0)	1156 (339)	14.76 (2.60)	9.2 (-12.7)
	2	5 (-15)	1 (-17)	75 (24)	0.5 (0.0025)	1212 (355)	14.78 (2.60)	5.2 (-14.9)
	3	155 (68)	80 (27)	74 (23)	0 (0)	-1155 (-338)	13.88 (2.44)	132.5 (55.8)
	4	155 (68)	91 (33)	74 (23)	0.5 (0.0025)	-960 (-281)	13.63 (2.40)	116.3 (46.8)
	5	154 (68)	100 (38)	74 (23)	1.5 (0.0076)	-953 (-279)	13.56 (2.39)	116.3 (46.8)
	1a*	5 (-15)	1 (-17)	75 (24)	0.5 (0.0025)	1111 (326)	15.61 (2.75)	8.4 (-13.1)
	4a*	151 (66)	90 (32)	76 (24)	0.5 (0.0025)	-902 (-264)	12.75 (2.25)	113.1 (45.1)
R-38 Batts	1 *	2 (-17)	0 (-18)	76 (24)	0 (0)	706 (207)	27.60 (4.86)	3.6 (-15.8)
	2	0 (-18)	-2 (-19)	76 (24)	0.5 (0.0025)	731 (214)	27.64 (4.87)	0.4 (-17.6)
	3	155 (68)	80 (27)	75 (24)	0 (0)	-633 (-186)	28.32 (4.99)	140.4 (60.2)
	4	153 (67)	91 (33)	76 (24)	0.5 (0.0025)	-483 (-142)	25.56 (4.50)	115.3 (46.3)
	5	152 (67)	101 (38)	76 (24)	1.5 (0.0076)	-480 (-141)	25.25 (4.45)	112.7 (44.8)

* Repeat tests performed after tests on R-38 insulation.
** Negative heat flows indicate heat is flowing into the space below the ceiling.
*** These results apply specifically to the size and shape of attic actually tested. Extrapolation to full-size attics requires consideration of edge heat flow effects as discussed in the text.

TABLE 7

Comparison of Results of Steady-State Attic Experiments
With Predictions of Finite-Difference Models

	Test	Mean Temperature, °F (°C)	R-Value, Percent Difference (Predicted-Measured)	Ceiling Heat Flow, Percent Difference (Predicted-Measured)
R-0	1	55.9 (13.3)	-10.8	-8.1
	2	47.4 (8.6)	-19.3	-9.1
	3	86.4 (30.2)	-8.0	0.3
	4	85.8 (29.9)	-12.8	5.9
	5	85.8 (29.9)	-14.0	-0.4
R-11	1	41.5 (5.3)	14.0	-11.4
	2	39.2 (4.0)	11.7	-10.2
	3	109.2 (42.9)	-18.5	33.7
	4	99.8 (37.7)	2.0	9.5
	5	100.8 (38.2)	-2.9	10.7
R-19	1	42.1 (5.6)	0.3	0.2
	2	40.8 (4.9)	0.8	-0.9
	3	107.9 (42.2)	-2.3	10.9
	4	102.8 (39.3)	-0.6	14.7
	5	101.4 (38.6)	-1.9	11.8
	1a	41.8 (5.4)	-5.1	4.9
	4a	100.4 (38.0)	6.9	4.1
R-38	1	40.0 (4.4)	-1.3	1.0
	2	38.7 (3.7)	-0.8	0.5
	3	110.0 (43.3)	-0.4	3.8
	4	101.2 (38.4)	6.3	5.0
	5	99.8 (37.7)	1.9	5.2

TABLE 8

Comparison of Results of Steady-State Attic Experiments
With Predictions of Overall Attic Models

		Ceiling Heat Flow, Percent Difference (Predicted-Measured)				Attic Air Temperature, °F (°C), (Predicted-Measured)							
	Test	OSU-EPRI	OCF-2	Air Well-Mixed	Air Not Well-Mixed	OSU-EPRI		OCF-2		Air Well-Mixed		Air Not Well-Mixed	
R-0	1	-8.4	1.8	-1.7	-1.7	-1.9	(-1.1)	-5.9	(-3.3)	0.6	(0.3)	0.6	(0.3)
	2	-19.1	-14.7	-11.8	-7.2	5.5	(3.1)	0.9	(0.5)	4.1	(2.3)	0.4	(0.2)
	3	-23.2	2.5	10.3	10.3	4.3	(2.4)	2.7	(1.5)	5.3	(2.9)	5.3	(2.9)
	4	-18.8	12.2	21.3	20.0	3.1	(1.7)	2.1	(1.2)	1.1	(0.6)	-0.2	(-0.1)
	5	-14.5	-1.9	8.2	8.4	1.8	(1.0)	3.1	(1.7)	3.1	(1.7)	3.3	(1.8)
R-11	1	-4.7	-3.4	-11.3	-11.3	-0.2	(-0.1)	-1.3	(-0.7)	0.3	(0.2)	0.3	((0.2)
	2	-2.3	-2.4	-9.9	-9.3	1.0	(0.6)	0.0	(0.0)	-0.5	(-0.3)	-1.6	(-0.9)
	3	2.2	13.5	33.0	33.0	4.4	(2.4)	-0.4	(-0.2)	5.5	(3.1)	5.5	(3.1)
	4	-15.2	5.7	18.2	11.5	8.7	(4.8)	4.4	(2.4)	3.5	(1.9)	-0.9	(-0.5)
	5	-23.1	3.3	16.5	10.9	0.8	(0.4)	-1.9	(-1.1)	-3.2	(-1.8)	-7.0	(-3.9)
R-19	1	1.5	2.3	-1.3	-1.3	-0.6	(-0.3)	-1.3	(-0.7)	-0.1	(-0.1)	-0.1	(-0.1)
	2	0.9	1.1	-2.4	-1.7	0.5	(0.3)	-0.2	(-0.1)	-0.5	(-0.3)	-1.4	(-0.8)
	3	-10.6	-3.4	11.3	11.3	5.8	(3.2)	1.1	(0.6)	6.8	(3.8)	6.8	(3.8)
	4	-15.2	3.0	14.9	8.6	7.4	(4.1)	2.7	(1.5)	1.9	(1.1)	-3.1	(-1.7)
	5	-25.5	-1.5	10.5	5.0	0.4	(0.2)	-2.6	(-1.4)	-3.9	(-2.2)	-8.1	(-4.5)
	1a	9.6	9.7	6.1	6.1	-2.4	(-1.3)	-3.3	(-1.8)	-3.6	(-2.0)	-3.6	(-2.0)
	4a	-18.0	-0.4	10.8	4.7	7.8	(4.3)	0.3	(0.2)	2.6	(-1.4)	-2.1	(-1.2)
R-38	1	-4.7	-4.1	-1.1	-1.1	0.1	(0.1)	-0.3	(-0.2)	0.4	(0.2)	0.4	(0.2)
	2	-4.3	-4.1	-1.5	-1.4	0.2	(0.1)	-0.2	(-0.1)	-0.5	(-0.3)	-1.0	(-0.6)
	3	-13.0	-9.5	3.5	3.5	2.3	(1.3)	-2.4	(-1.3)	3.1	(1.7)	3.1	(1.7)
	4	-14.9	0.4	13.1	6.8	9.0	(5.0)	4.4	(2.4)	3.4	(1.9)	-1.8	(-1.0)
	5	-25.0	-3.5	12.2	6.8	4.2	(2.3)	1.3	(0.7)	0.0	(0.0)	-4.3	(-2.4)

TABLE 9

Comparison of Results of Transient Attic Experiments
With Predictions of Overall Attic Models

Test		Integrated Ceiling Heat Flow,* Percent Difference (Predicted-Measured)			
		OSU-EPRI	OCF-2	Air Well-Mixed	Air Not Well-Mixed
R-0	Winter	-10.3	-1.2	-4.8	-4.8
	Summer	-28.0	2.2	-0.5	0.7
R-11	Winter	-6.5	-5.0	-11.8	-11.8
	Summer	-11.7	15.1	26.5	17.2
R-19	Winter	-6.4	-4.5	-4.6	-4.0
	Summer	-12.4	9.8	19.1	10.8
R-38	Winter	-11.6	-10.8	-4.2	-4.2
	Summer	-13.1	6.8	16.4	5.6

* Integrated ceiling heatflow is equal to the sum of the absolute values of the hourly ceiling heatflows over the last 48 hours of the transient test (two complete daily cycles).

TABLE 10

Form of Energy Factor Regression Equations

Heating: $E = HDD\,[A + B\times BP + C\times HSLOPE + D\times \ln(U) + E\times U + F\times BP\times HSLOPE + G\times BP\times \ln(U) + H\times BP\times U + I\times \ln(U)/BP + J\times HSLOPE\times U + K\times U\times \ln(U) + L\times BP^2 + M\times U^2 + N/(CDD+HDD) + O\times HSLOPE/(CDD+HDD) + P/BP + Q\times HSLOPE\times BP/(CDD+HDD) + R\times BP/(CDD+HDD) + S\times \ln^2(U)]$

Cooling: $E = A + B\times CDD + C\times BP + D\times CSLOPE + E\times U + F\times CDD\times BP + G\times CDD\times CSLOPE + H\times CDD\times U + I\times BP\times CSLOPE + J\times BP\times U + K\times CSLOPE\times U + L\times CDD^2 + M\times BP^2 + N\times BP^3 + O\times CDD/(CDD+HDD) + P\times[CDD/(CDD+HDD)]^2 + Q\times COC + R\times COC^2 + S\times COC\times CDD/(CDD+HDD) + T/BP^2 + V\times U/BP + W/(U\times CH^2) + X\times BP/(U\times CH^2) + Y\times BP/CH^2 + Z/CH^2 + AA/(U\times CH)^2 + BB\times(BP/(U\times CH))^2 + CC\times(BP/CH)^2 + DD\times(BP/CH)^2/U + EE\times BP/(U\times CH)^2$

E = energy factor, kW-hr/ft²
U = thermal transmittance, Btu/(hr-ft²-°F)
BP = house balance point, °F
HDD = heating degree days based on house balance point
CDD = cooling degree days based on house balance point
HSLOPE = (HDD(65)-HDD(60))/(HDD(65)-HDD(45)), where HDD indicates the number of heating degree days to the base in parentheses
CSLOPE = (CDD(65)-CDD(60))/(CDD(65)-CDD(45)), where CDD indicates the number of cooling degree days to the base in parentheses
COC = CDD(65)/CDD(45)
CH = cooling hours over 80°F
A,...,T,V,...,Z,AA,...,EE = regression constants

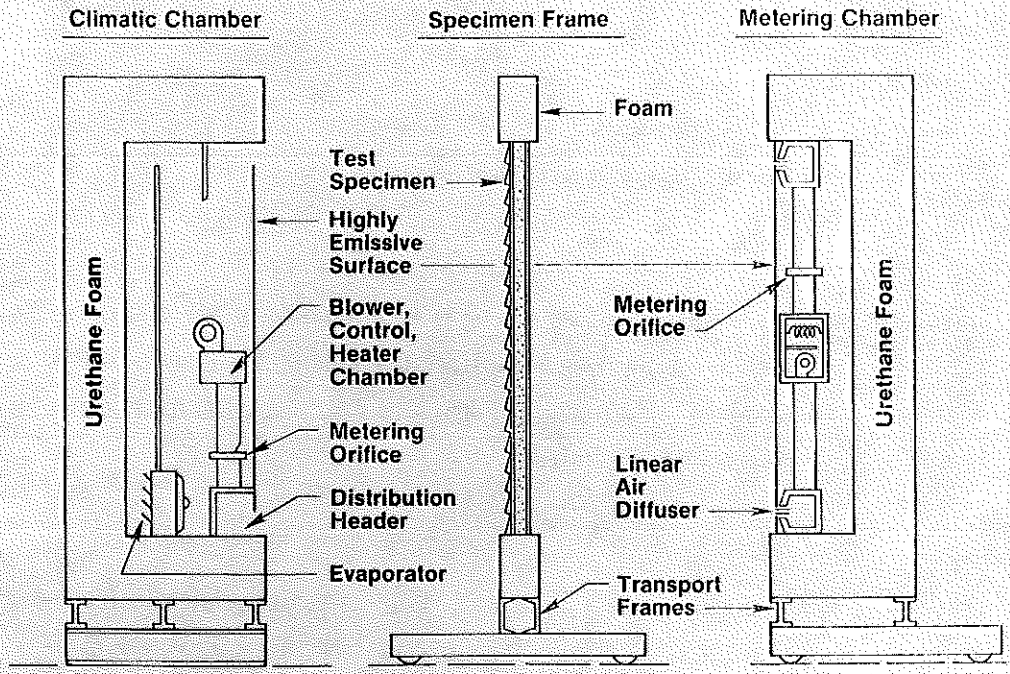

Figure 1. Schematic diagram of the calibrated hot box

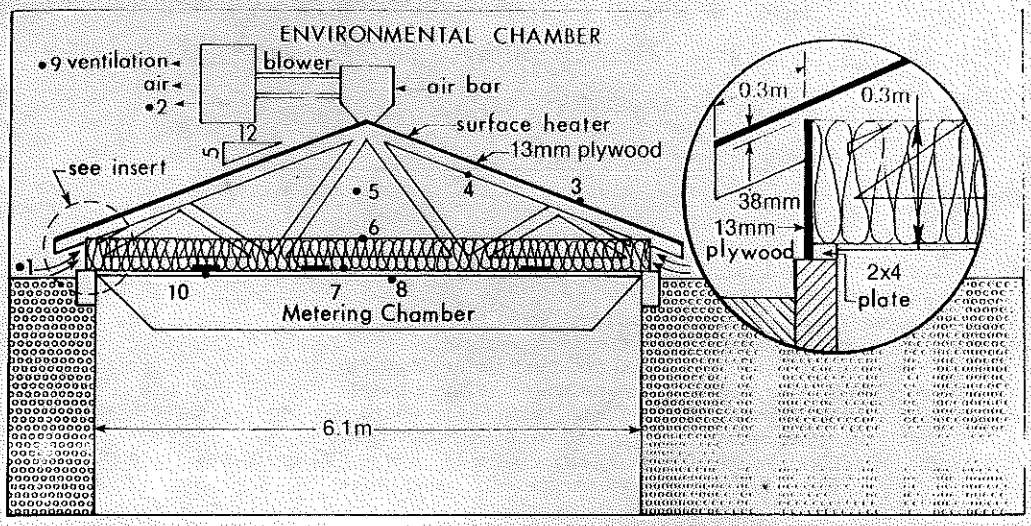

- •1 Inlet air temperature
- •2 Discharge air temperature
- •3 Top of roof surface temperature
- •4 Deck bottom temperature
- •5 Mid height air temperature
- •6 Top surface of insulation temperature
- •7 Ceiling/insulation interface temperature
- •8 Ceiling surface temperature
- •9 Ventilation rates
- •10 Heat flux through the ceiling

Figure 2. Attic module and instrumentation

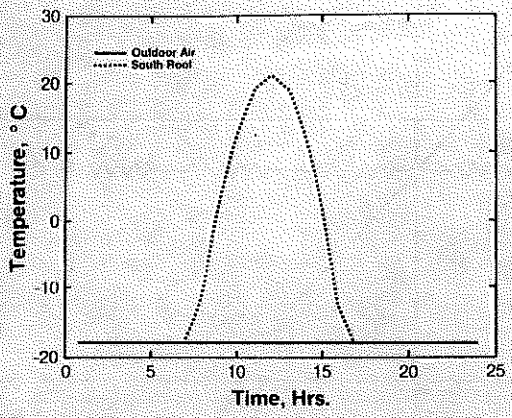

Figure 1. Attic winter transient temperature conditions

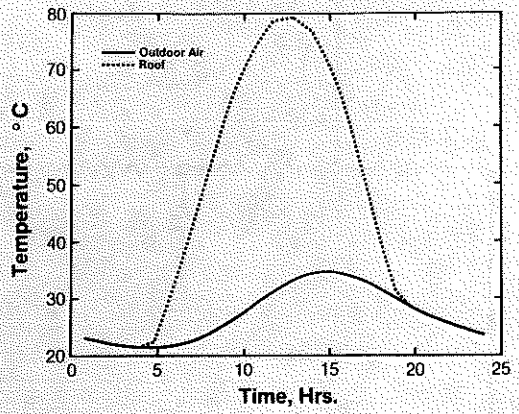

Figure 4. Attic summer transient temperature conditions

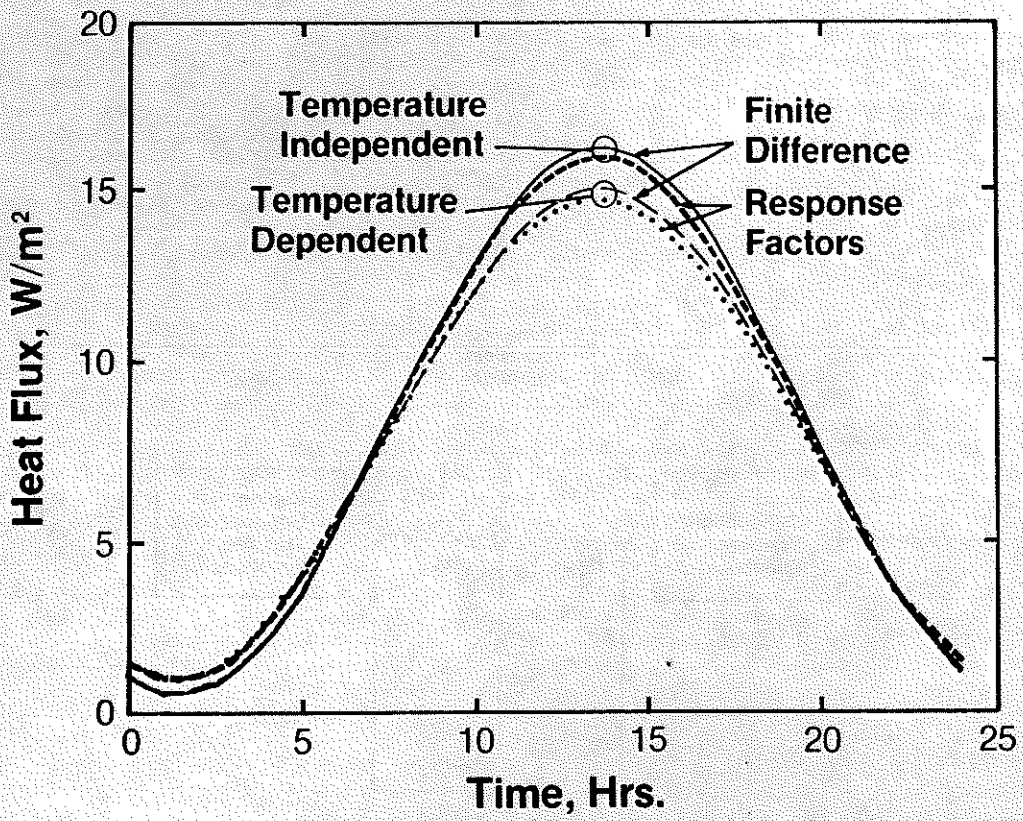

Figure 5. Comparison of calculation methods for inside surface heat flux for insulated frame wall

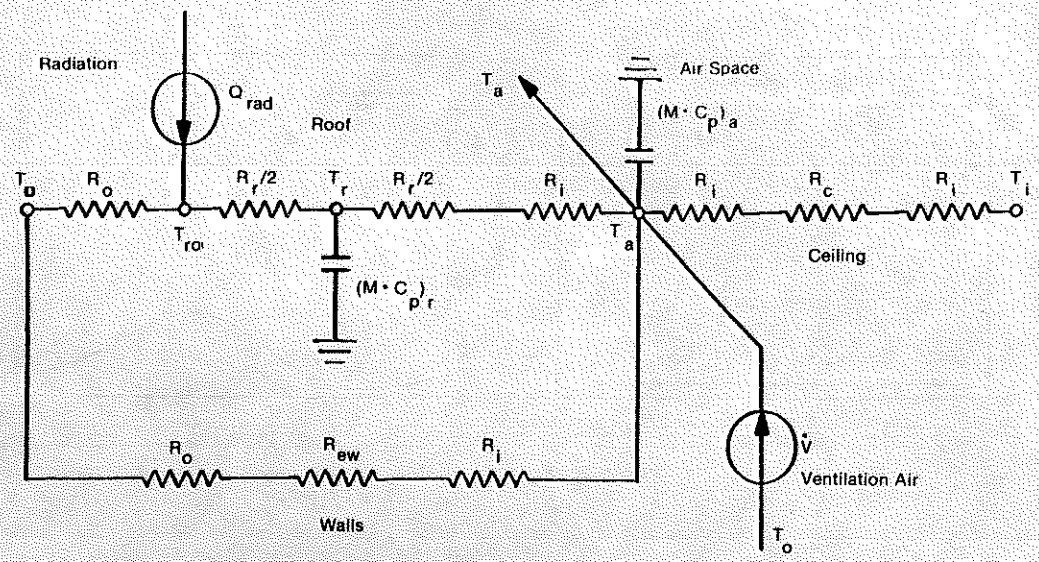

Figure 6. Schematic of OSU-EPRI attic model

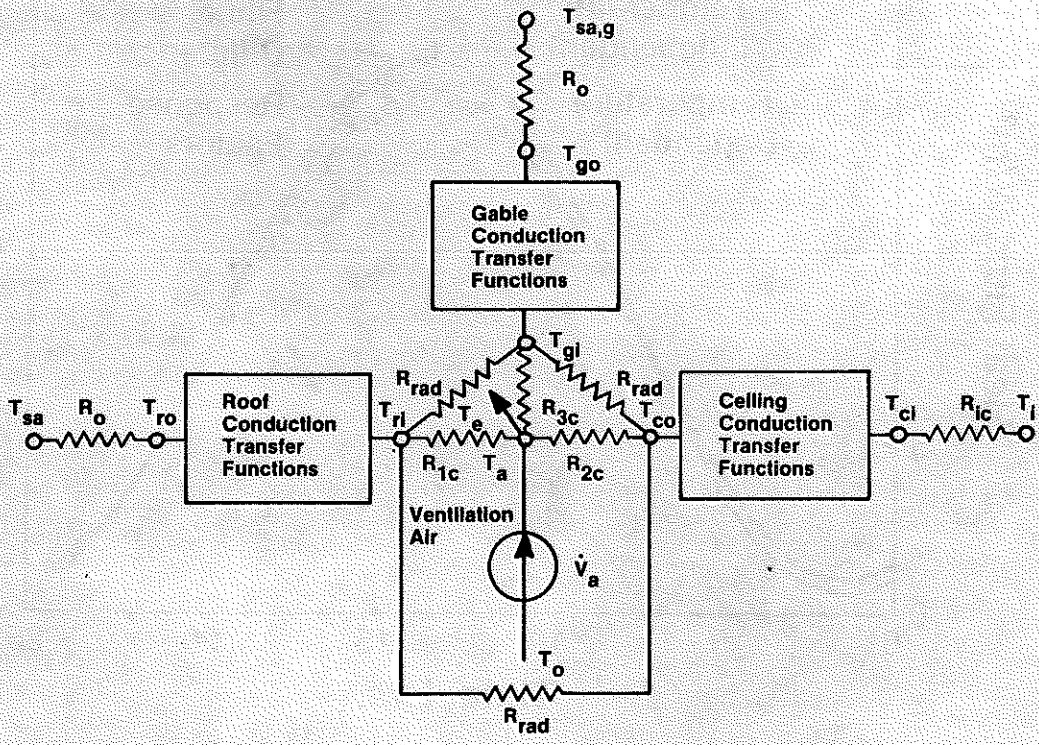

Figure 7. Schematic of OCF attic model

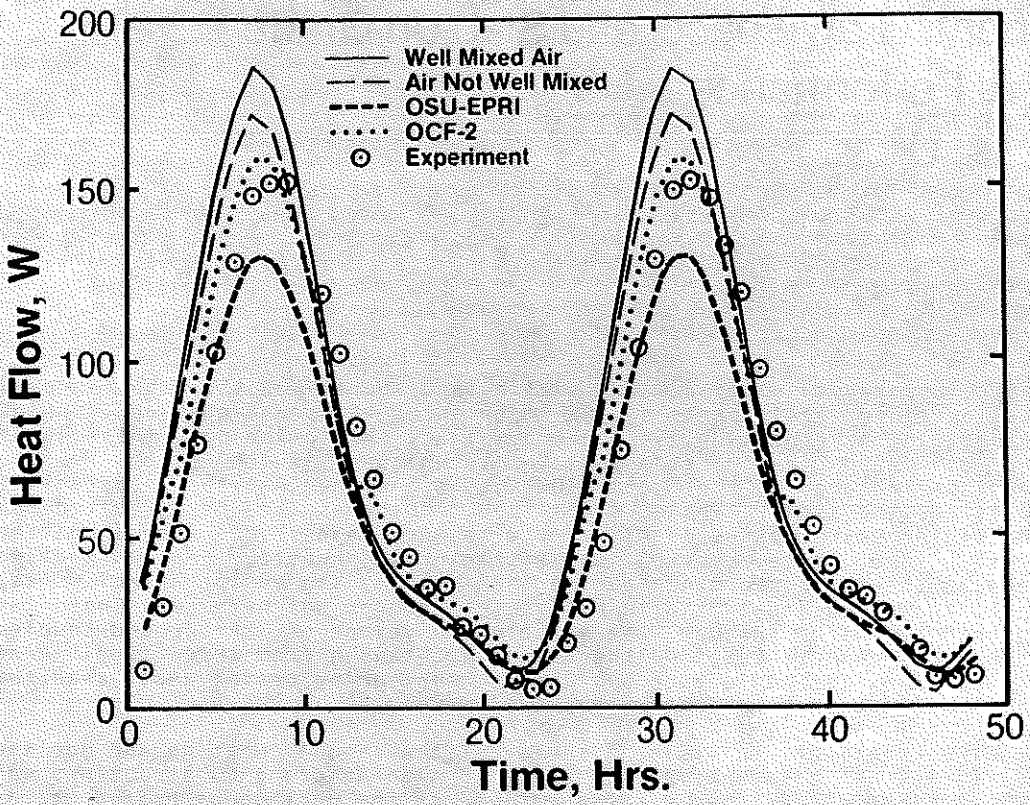

Figure 8. Ceiling heat flow for R-38 attic summer transient test

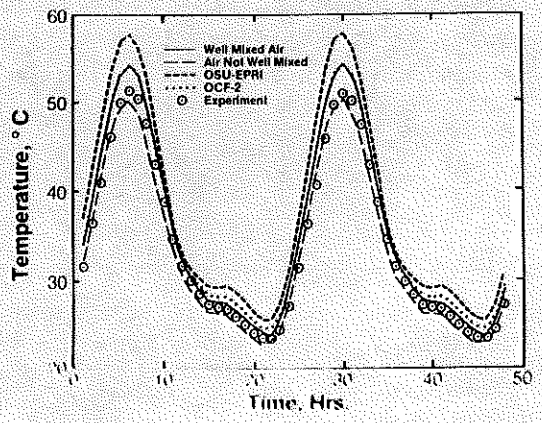

Figure 9. Ceiling temperature for R-38 attic summer transient test

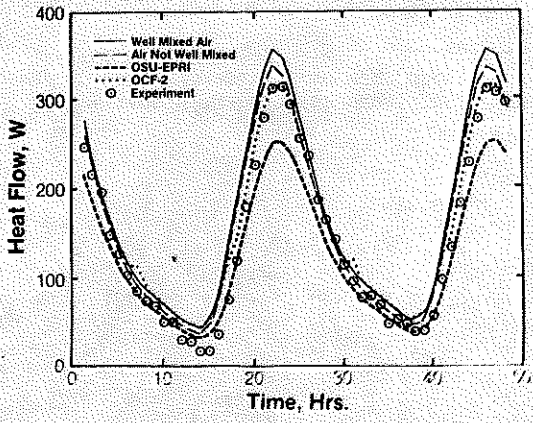

Figure 10. Ceiling heat flow for R-19 attic summer transient test